UNIVERSITY OF MISKOLC
FACULTY OF MECHANICAL ENGINEERING AND INFORMATICS

MODELING, SIMULATION AND ENERGY CONSUMPTION ANALYSIS OF THE CUTTING FORCE OF BATTERY-POWERED HANDHELD JIGSAWS

PhD DISSERTATION
THESIS BOOKLET

Prepared by

Sándor Apáti
Mechanical Engineer (MSc)

SÁLYI ISTVÁN DOCTORAL SCHOOL OF MECHANICAL ENGINEERING SCIENCES
RESEARCH FIELD: DESIGN OF MACHINES AND STRUCTURES
RESEARCH GROUP: DESIGN OF MACHINE TOOLS

Head of the Doctoral School:
Prof. Dr. Gabriella Bognár Vadászné
DSc, University Professor

Head of the Research Group:
Dr. György Hegedűs
Associate Professor

Supervisor:
Dr. György Hegedűs
Associate Professor
Co-Supervisor:
Dr. Sándor Hajdu
Associate Professor

Miskolc
2025

Table of Contents

1. Introduction

The energetic and dynamic analysis of battery-powered handheld jigsaws is of paramount importance for modern industrial applications and sustainable development. These tools enable precise and flexible machining of various materials (wood, metal, plastic); however, their operation can involve significant energy losses, primarily due to dynamic cutting forces and tool–material interactions. These losses not only increase energy consumption but also degrade cutting quality and reduce the lifespan of the tool.

The aim of my research is to investigate these issues from the perspectives of measurement, modeling, and control, with a particular focus on the interrelation between cutting forces, vibrations, and energy consumption. To achieve this, a custom-developed test bench system was employed, capable of accurately measuring cutting forces in real time and minimizing the effects of dynamic disturbances in the system. During the experiments, the cutting behavior of various materials (oak, acacia, aluminum, metamid) was examined, with special attention to the influence of material properties such as density and elasticity.

Force fluctuations and vibrations occurring during the cutting process can cause instability; therefore, my goal was to develop a model-based approach capable of accurately describing these phenomena. In the course of the research, both linear and nonlinear cutting force models were developed within the Simscape environment. These models, after optimization-based fine-tuning, proved suitable for predicting energy consumption. High inrush currents commonly observed during the start-up of DC motors pose an additional challenge, as they negatively impact battery life and motor reliability. With the omission of gearboxes, the role of control becomes more critical, since load fluctuations act directly on the motor, particularly when cutting hardwoods or layered materials.

To address these challenges, I applied sliding mode control methods, which can robustly handle load variations and ensure stable operation. One of the key advantages of sliding mode control is its ability to effectively reduce inrush currents during start-up, improve energy efficiency, and extend battery runtime. Consequently, the handheld jigsaw becomes more reliable and durable, especially in industrial applications.

The objective of this dissertation is to develop a comprehensive, integrated methodology for measurement, modeling, and control, contributing to the energy-efficient and stable operation of battery-powered jigsaws.

2. Presentation of the Electromechanical Model

To analyze the operation of the jigsaw, an electromechanical model was developed that uniformly addresses the interactions between the motor, the scotch-yoke mechanism, and the cutting process. The aim is to enable accurate prediction of cutting forces, energy consumption, and dynamic behavior, as well as to explore potential control strategies. To

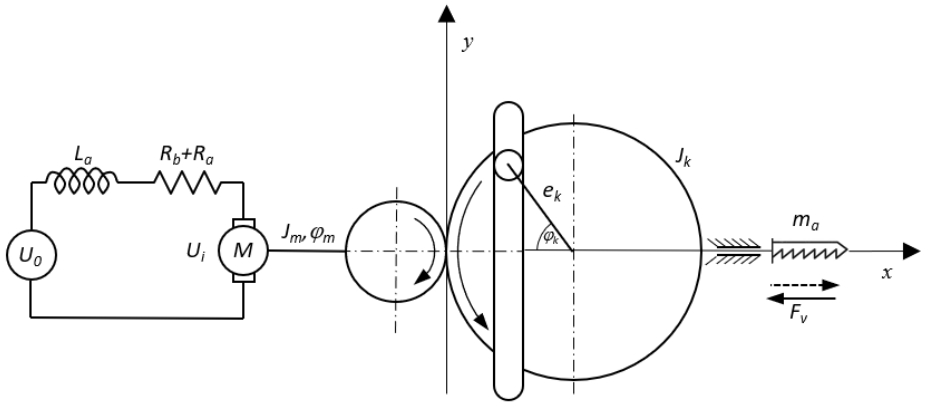

Figure 2.1: Electromechanical model of the handheld jigsaw [S4].

derive the equations of motion, the second-order Lagrange equation was applied, which takes the general form:

$$\frac{d}{dt}\left(\frac{\partial L}{\partial \dot{q}_i}\right) - \frac{\partial L}{\partial q_i} = Q_i, \tag{2.1}$$

where $q_1 = q(t)$ denotes the electric charge, and $q_2 = \varphi_m(t)$ the angular position of the motor shaft. Substituting into the system, the electromechanical equations become:

$$U_0 = L_a\ddot{q} + R_a\dot{q} + k_e\dot{\varphi}_m, \tag{2.2}$$

$$J_{eq}(\varphi_m)\ddot{\varphi}_m + \frac{1}{2}J'_{eq}(\varphi_m)\dot{\varphi}_m^2 = k_m\dot{q} - F_v e_k k_{mk}\sin\left(k_{mk}\varphi_m\right) - b\dot{\varphi}_m. \tag{2.3}$$

Due to the nonlinear characteristics of the system, numerical solutions were obtained using a fourth-order Runge–Kutta method with adaptive step size. The model provides a detailed insight into the dynamics of the cutting process, serving as a foundation for subsequent control and optimization tasks.

3. Experimental Measurements

Measuring the cutting force of an electric handheld jigsaw poses a significant challenge. My first task was to design a measurement system capable of performing accurate cutting force measurements.
The test rig was designed to be suitable for machining different materials, such as acacia wood, aluminum, and metamid. For all materials, identical experimental parameters were applied—including feed rate and cutting speed—to ensure the consistency of the investigations. This unified approach enabled a direct comparison of cutting force behavior across different materials.
The structure of the measurement system is shown in Figure 3.1.

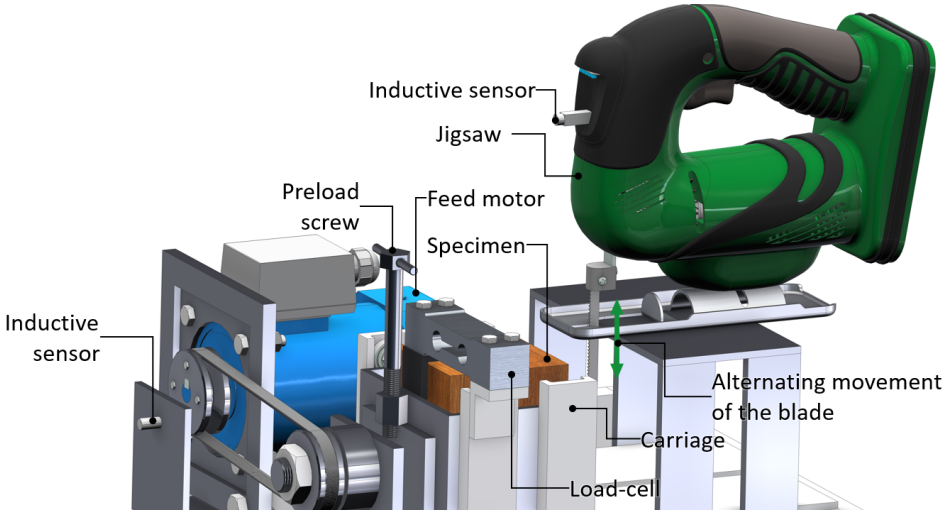

Figure 3.1: Structure of the measurement system [S4].

To minimize vibrations, the carriage was equipped with a preloaded spindle shaft that generated a preload force (F_c) between the force sensor and the workpiece holder. Before each measurement, a workpiece of dimensions $80 \times 80 \times 80$ mm was fixed into the carriage. In the case of wooden specimens, the grain direction was always oriented perpendicular to the feed direction to ensure that the cut was consistently perpendicular to the grain, thus guaranteeing the repeatability of the results [1, 2].
Once the workpiece was secured, the handheld jigsaw was activated. The device was equipped with an inductive sensor that detected the top dead center of the scotch-yoke mechanism and transmitted a signal to the data acquisition system. This sensor was used exclusively at the start-up phase to measure the initial speed of the unloaded motor. The actual angular velocity under load was determined using Fourier analysis. This solution allowed the measurement system to operate without disassembling or modifying the jigsaw.
The feed motion was provided by a three-phase motor equipped with a frequency inverter.

An inductive proximity sensor detected the passage of 6 mm diameter bolts placed equidistantly around the pulley of the drive motor, enabling precise determination of the motor's rotational speed.
During cutting, the carriage tends to move upward as a result of the cutting force. This motion is resisted by the force sensor, which records the reaction force—thereby measuring the actual cutting force. This measurement setup provides accurate data on the dynamics of the cutting process. According to Figure 3.2b, several forces act on the

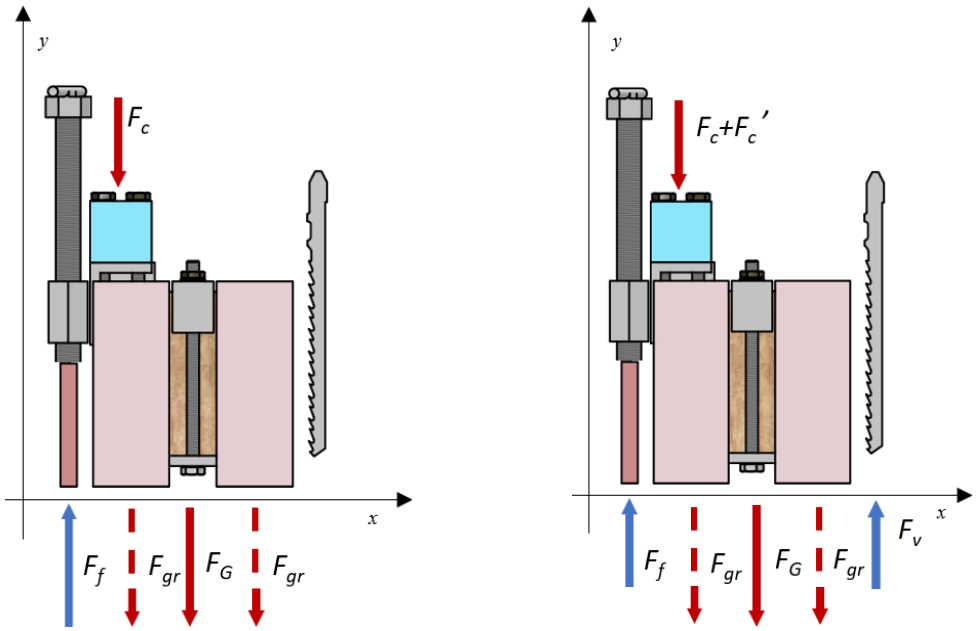

(a) Forces under preload condition.

(b) Forces during cutting.

Figure 3.2: Forces acting on the workpiece and the force sensor [S4].

system during sawing, including the cutting force (F_v), the gravitational force (F_G), the preload force (F_f), and the forces acting on the force sensor (F_c and F_c'). Figure 3.2a shows the preloaded state of the measurement system, to which the following static equilibrium equation can be applied:

$$\sum F_y = 0 = F_f - F_c - F_G - F_{gr}. \tag{3.1}$$

From the configuration shown in Figure 3.2b, the equilibrium equation for the cutting process can be written as:

$$\sum F_y = 0 = F_f + F_v - (F_c + F_c') - F_G - F_{gr}. \tag{3.2}$$

Based on Equation (3.2), and considering the static balance of Equation (3.1), the cutting force can be expressed as:

$$F_v = F_c' + F_{gr}. \tag{3.3}$$

It is evident that in the preloaded (zeroed) state of the measurement system, the force sensor directly measures the cutting force. This is because the additional force measured by the sensor (F_c') is exactly equal to the difference between the cutting force (F_v) and the frictional resistance (F_{gr}). This measurement configuration ensures that cutting force measurements remain accurate and reproducible throughout the entire sawing process.

3.1. Determination of the Specific Cutting Force

As the first step of the cutting force measurements, the so-called direct cutting force was recorded using a force sensor during the cutting process. Figure 3.3 shows the cutting force diagram obtained for an oak sample under the following measurement parameters:

- initial unloaded crankshaft speed: 18.41 1/s,
- feed rate: $3.93\,\mathrm{mm\,s^{-1}}$,
- blade deflection: 1.5 mm.

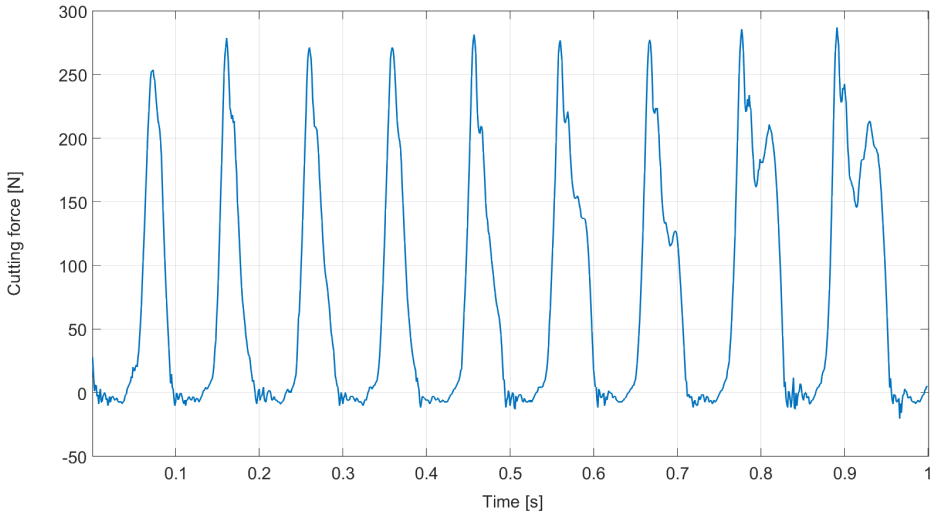

Figure 3.3: Cutting force diagram for oak workpiece.

In parallel with the measurement shown in Figure 3.3, the feed force was also determined from the current drawn by the feed motor. The normal force during feed was found to be $F = 18.3\,\mathrm{N}$, which is at least one order of magnitude smaller than the vertical cutting force. In practical use, this feed force is applied manually by the operator. The amplitude spectrum derived from the cutting force measurement shown in Figure 3.3 is illustrated in Figure 3.4, generated using Fast Fourier Transform (FFT) [3].

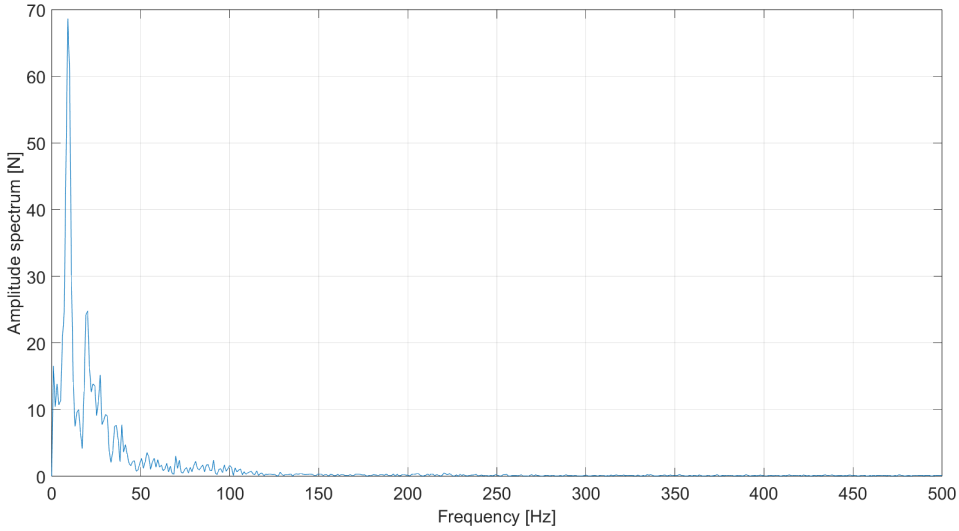

Figure 3.4: Typical amplitude spectrum of the cutting force for oak sample.

Figure 3.3 presents the diagram of the specific cutting force, calculated using the previously described method for the oak specimen. The negative values observed in the

diagram do not reflect actual cutting forces, but result from transient distortions caused by the internal elasticity of the measuring system and elastic deformations due to the preload. These are inherent characteristics that must be considered when evaluating measurement accuracy. Extremely high values are attributed to the inhomogeneous nature of the wood sample. As noted in [4], the cutting force depends on both the feed rate and the cutting speed. This implies that higher crankshaft speeds should result in lower cutting forces. According to [1, 5, 6], friction-induced heating during sawing softens the fibers near the cutting edge, thereby facilitating the cutting process.

Table 3.1: Specific cutting forces [N/mm²] for various feed rates and initial/actual crankshaft speeds

Feed [mm/s]	**Initial speed [1/s]**	**10.52**	**13.15**	**15.78**	**18.41**	**21.04**	**23.67**	**26.30**	**28.93**	**31.56**	**34.19**	**36.82**	**39.45**	**42.08**
	Actual speed [1/s]	1.01	1.01	1.01	7.07	12.12	12.12	14.14	16.16	21.21	25.25	25.28	30.30	34.30
3.93		0	0	0	1952	6554	2560	2943	5735	3296	2605	4474	5824	4328
5.49		0	0	0	2270	2362	3435	3887	4054	4531	4426	4584	5333	2940
6.63		0	0	0	1834	2516	2801	2879	3341	3974	3602	4392	4443	2117

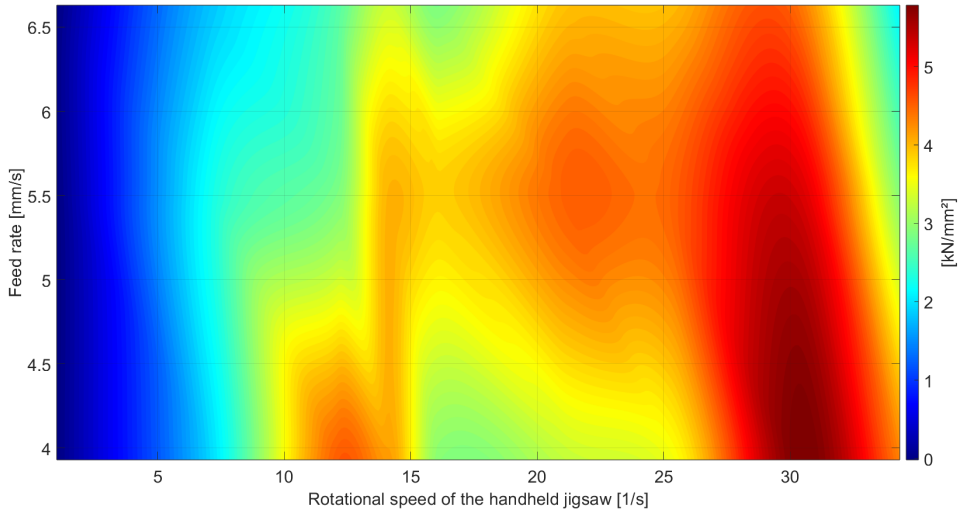

Figure 3.5: Specific cutting forces based on the data from Table 3.1.

Multiple series of measurements were performed, each repeated three times with various feed rates and motor speeds. The measured values presented in Table 3.1 are visualized in the surface plot of Figure 3.5. It can be seen that the tests for oak wood were conducted at 13 different actual crankshaft speeds and 3 different feed rates. The diagram illustrates how the cutting force of the jigsaw varies as a function of crankshaft angular velocity and feed speed.

The horizontal axis represents angular velocity [s^{-1}], the vertical axis shows feed rate [$mm\,s^{-1}$], while the color map indicates cutting force in [$kN\,mm^{-2}$]. Based on the diagram, it is observed that at low angular velocities (4–10 s^{-1}), the cutting force remains low, suggesting decreased cutting efficiency and a "jerky" blade motion. As the angular velocity increases, the cutting force gradually rises, with a force peak occurring around 18–20 s^{-1} angular speed and 5–6 $mm\,s^{-1}$ feed rate.

The optimal operating zone appears to lie in the range of approximately 20–25 s^{-1} angular velocity and 5.5–6 $mm\,s^{-1}$ feed rate, where the cutting force is high but remains below a critical level, enabling efficient and stable cutting. The highest cutting forces were observed in the 25–30 s^{-1} range, which allows for faster cutting but imposes in-

creased mechanical stress on the tool components, reducing their lifespan.
Based on the data, the operation of the jigsaw can be optimized by controlling angular velocity and feed rate within the identified effective zone. This insight supports further development efforts such as load-dependent automatic speed control or the implementation of intelligent control systems that adapt cutting parameters based on resistance, improving both efficiency and tool longevity.
The anomalies identified in the measurements, such as peak cutting forces and occasional negative values, are attributed to multiple factors related to the complex dynamics of the cutting process.

3.2. Current Measurement During the Cutting Force Test

The results of the current measurements related to the cutting force test are shown in Figure 3.6. The current was measured using a Fluke 124B oscilloscope and current clamp, while the cutting force was measured via a LabVIEW-based system. Synchronization of the two time series was performed during post-processing.

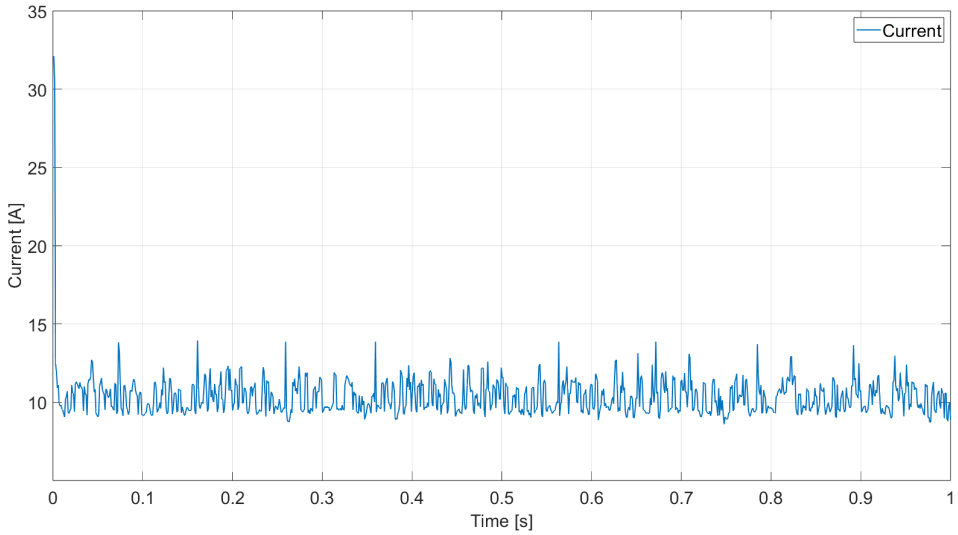

Figure 3.6: Current–time diagram measured during the cutting force test.

The synchronization reference point was determined by the current and force peaks observed at the onset of cutting. The sampling frequency for both measurement instruments was 1 kHz. A starting peak of approximately 32 A can be observed on the current curve, after which the current stabilizes in the range of 8–14 A. These fluctuations are attributed to material inhomogeneity, variations in feed rate, and mechanical kickbacks.
Based on the processed data, the average current ($\langle I \rangle$), the energy consumption (E), and the expected battery runtime (T_{accu}) were determined. The current–time diagram effectively characterizes the load behavior of the jigsaw and highlights the dynamic nature of the cutting process.

4. Prediction of Battery Runtime of Jigsaws Using a Linear Cutting Force Model

Improving the energy efficiency and dynamic stability of handheld jigsaws presents a significant challenge due to nonlinear cutting forces, material properties, and vibrations. The dynamic forces arising during the cutting process not only increase energy consumption but also introduce instability and vibrations, thereby degrading cutting quality and reducing the machine's lifespan.
Conventional models often fail to adequately address these complex factors, limiting their applicability in accurately predicting battery runtime. In this research, a linear cutting force model-based approach was employed, which—despite its simplicity—provides an effective estimation of the energy demand of the cutting process. This enables operational optimization aimed at extending the battery runtime.

4.1. Simscape Model with Real Cutting Force

Simscape is an integrated simulation environment that enables the realistic modeling and analysis of electromechanical systems. The platform supports the direct coupling of electrical and mechanical components, ensuring accurate representation of the full system dynamics. Its built-in libraries offer components such as motors, dampers, springs, and electrical elements (resistors, inductors, capacitors), all of which can be parameterized based on their physical properties (e.g., EMF, resistance, inertia, damping).
With these components, the loaded operation of DC motors and the interaction between mechanical and electrical subsystems can be effectively analyzed [7]. The cutting force as a function of angular displacement accurately describes the periodic behavior of the jigsaw and provides realistic force inputs for the simulation [8].
The model built in the Simscape environment integrates the dynamics of the motor, gear system, and scotch-yoke mechanism. The rotary motion of the DC motor is converted into an oscillating motion by the mechanism, resulting in the back-and-forth movement of the saw blade. The cutting force is applied based on an angle-dependent *1-D Lookup Table*, allowing precise mapping of the dynamic cutting process.

4.2. Simscape Model with Linear Cutting Force Approximation

By simulating the electromechanical system of the jigsaw using a linear cutting force approximation, the operating parameters of the system can be computed more quickly while still producing realistic results. The core of the model consists of a DC motor, a gear system, and a scotch-yoke mechanism, which converts rotary motion into reciprocating motion.

The cutting force is calculated using a linear damping model based on the velocity of the saw blade. Friction and switching blocks control the activation of the damping within the appropriate angular position range. The system's current and angular position sensors provide real-time data on current consumption and mechanical states, allowing for the analysis of the dynamic behavior of the cutting process.

4.3. Simulation of Battery Runtime Using Simscape Models

After completing the optimization process, further simulations were conducted using the optimal damping coefficient to estimate the battery runtime of the handheld jigsaw. The energy source of the system is a battery, whose *State of Charge* (SOC) is continuously monitored during the simulation. The battery current is regulated by a *DC-DC* converter, which ensures the appropriate voltage and current supply to the *DC* motor. This converter is essential for energy efficiency calculations and also allows the simulation of the motor's actual PWM-controlled input voltage.
Battery behavior is modeled using the *Battery* block, which supports two simulation approaches. When the battery capacity parameter is set to *Infinite* (*Battery Charge Capacity: Infinite*), the block models the battery as a series internal resistance and a constant voltage source. This simplified approach is ideal when the variation in the battery's state of charge is not critical. In contrast, when the battery capacity is defined as *Finite* (*Battery Charge Capacity: Finite*), the block models the battery as an internal resistance and a voltage source dependent on the SOC. In this case, the output voltage is calculated using the following equation:

$$V = V_{nom} \frac{\text{SOC}}{1 - \beta(1 - \text{SOC})}, \tag{4.1}$$

where V_{nom} is the nominal battery voltage, SOC represents the current State of Charge, and β is a parameter characterizing the battery's internal nonlinearity. This equation accurately models how the output voltage depends not only on the nominal voltage but also on the SOC. As the state of charge decreases, the voltage also declines, which is crucial for ensuring energy-efficient operation.
This detailed battery model allows the simulation to realistically represent the dynamics and behavior of an actual battery. These models are particularly suitable for the development of portable handheld jigsaws, where optimizing energy consumption and improving cutting quality are key objectives. By considering the impact of energy consumption on battery state of charge, the model enables the maximization of battery life while ensuring stable and reliable system operation. Thus, the model is not only suitable for research purposes but also extremely valuable for industrial applications, contributing to advancements in modern jigsaw design and development.
The system includes multiple sensors that provide real-time feedback on the system's operation. These include the *Current Sensor*, which measures motor current consumption; the *Force Sensor*, which captures the forces generated during cutting; and the *SOC Monitor*, which tracks the battery's state of charge and stops the simulation when critical levels are reached. Logical control components, such as a *Switch* block, manage the system's operational states. The *Switch* monitors the *SOC* and activates the *Stop Simulation* block when the SOC drops below a predefined threshold, thus preventing battery damage and ensuring safe operation.

In the simulation, it was assumed that a fully charged battery discharges down to an SOC level of 20%. The simulated battery runtime using the real cutting force model is:

$$t_{br} = 963\,\text{s}.$$

The simulated battery runtime using the linear cutting force model is:

$$t_{bl} = 927\,\text{s}.$$

The relative prediction error is:

$$e_r = \frac{t_{br} - t_{bl}}{t_{br}} = 0.037 = 3.7\%. \tag{4.2}$$

This relatively small error indicates that the linear cutting force model effectively approximates the real model and provides reliable estimates of battery runtime under realistic operating conditions.

4.4. Simulation Results

The behavior of motor current and cutting force was compared using both real and linear cutting force models. Figure 4.1 presents the current–time diagram showing the measured current, the simulated current based on the nonlinear (real cutting force) model, and the current from the model approximated with a linear damping coefficient over a 50 s interval. This duration covers more than 5% of the total simulation period, providing a solid validation basis for evaluating the model's reliability and accuracy.
The purpose of this comparison is to experimentally confirm the validity and practical applicability of the linear approximation model.

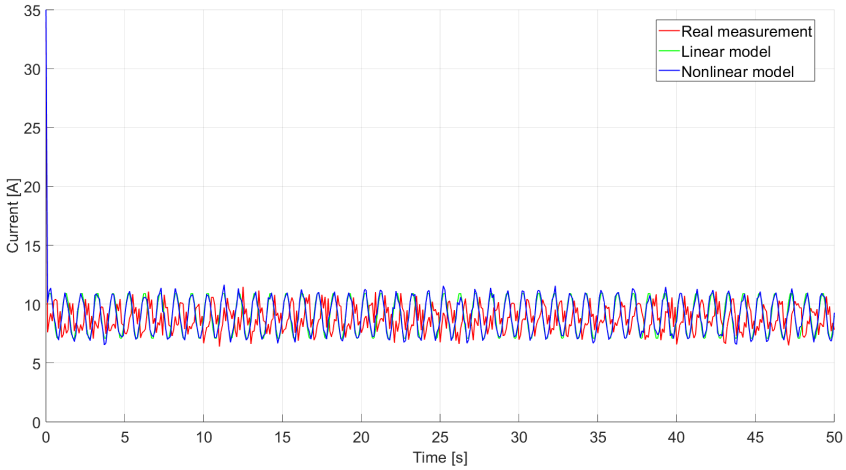

Figure 4.1: Comparison of motor current over a 50-second interval: real measurement, nonlinear cutting force model, and linear model.

Detailed analysis of the curves reveals that the measured current (red curve) closely matches the simulation using the real, nonlinear cutting force model (blue curve). The results from the linear model (green curve) also show good agreement with the real current, particularly in terms of temporal behavior, periodic structure, and average current levels.
The time evolution of the three current signals is well aligned; the waveforms remain in

phase, and the vibration dynamics exhibit significant similarity. This coherence confirms that the linear model with optimized damping is not only suitable for estimating energy consumption, but also capable of predicting the time-varying motor current with adequate precision—thereby accurately representing the system's fundamental electromechanical dynamics.
Minor discrepancies can be observed at force peaks; however, the overall agreement is strong, making the linear model suitable for runtime estimation and energy efficiency studies. The relative deviation in battery runtime is:

$$e_r = 0.037 = 3.7\%. \tag{4.3}$$

The Simscape-based model accurately describes the cutting process dynamics and the power supply behavior. Despite its simplicity, the optimized linear model effectively approximates real cutting conditions and provides a reliable foundation for the development of portable handheld jigsaws.
Figure 4.2 illustrates the time-dependent cutting force in both the real and linear models. This figure is crucial to the study as it highlights differences and similarities between the two models and evaluates the linear model's effectiveness in approximating real cutting forces.

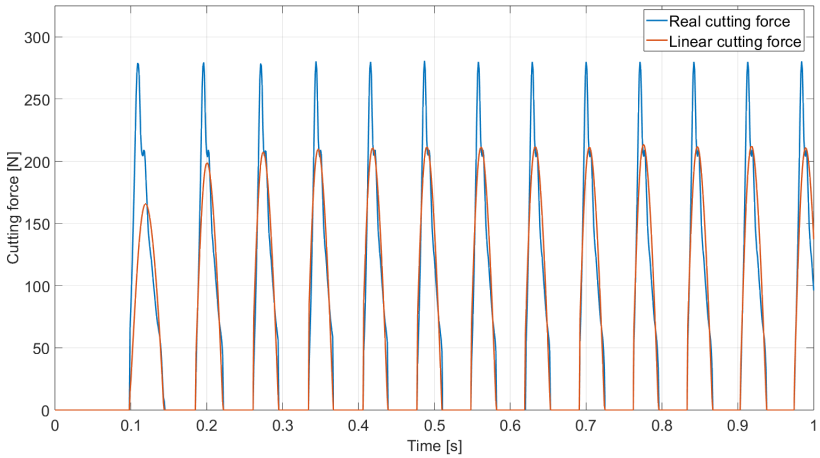

Figure 4.2: Comparison of cutting forces for real and linear models.

The plotted curves represent the actual measured cutting force $F_{\text{real}}(t)$, obtained through direct measurement during the operation of the handheld jigsaw, and the cutting force generated by the linear model $F_{\text{linear}}(t)$. The parameters of the linear model, particularly the damping coefficient, were optimized through an identification process to minimize discrepancies between real and simulated cutting forces.
This identification framework is based on an optimization block diagram that applies the *simulated annealing* algorithm to determine the optimal damping coefficient, ensuring the linear model closely follows the real cutting force.
Analysis of the cutting force–time diagram shows that the linear model approximates the behavior of the real cutting force reasonably well. Although some deviations are observed—especially at the force peaks—these are negligible in light of the model's simplicity. The overall agreement is strong, confirming the applicability of the linear model for realistic simulations.

4.5. Validation Based on the 50-Second Interval

To evaluate the reliability of the simulation model, the expected battery runtime was calculated not only for the full test period but also for a representative 50-second interval that aligns with the real measurement data. This time span is representative of the system's loading conditions and the periodic behavior of motor current and cutting force, thus providing a solid validation basis for assessing the accuracy of the model formulation. Based on the measurements and simulations, the following average current values were determined:

- Based on measured data:
$$\langle I_{\text{measured}} \rangle = 8.51\,\text{A},$$
- Based on the fitted linear model:
$$\langle I_{\text{lin}} \rangle = 7.77\,\text{A},$$
- Based on the nonlinear model:
$$\langle I_{\text{nonlin}} \rangle = 8.24\,\text{A}.$$

The battery capacity is $Q = 2.5\,\text{Ah}$, which equals 9000 As. During the simulation, the energy reserve decreases from 100% to 20%, meaning the usable charge is:

$$Q_{\text{usable}} = 9600\,\text{A s} \cdot 0.8 = 7200\,\text{A s}. \tag{4.4}$$

The expected runtime in each case can be calculated using the following expression:

$$T = \frac{Q_{\text{usable}}}{\langle I \rangle}. \tag{4.5}$$

The resulting runtimes for each model are as follows:

$$T_{\text{measured}} = \frac{7200\,\text{A s}}{8.51\,\text{A}} \approx 846.0\,\text{s}, \tag{4.6}$$

$$T_{\text{lin}} = \frac{7200\,\text{A s}}{7.77\,\text{A}} \approx 926.96\,\text{s}, \tag{4.7}$$

$$T_{\text{nonlin}} = \frac{7200\,\text{A s}}{8.24\,\text{A}} \approx 873.8\,\text{s}. \tag{4.8}$$

The relative deviation of the linear model compared to the measured value:

$$\Delta_{\text{lin}} = \frac{926.96\,\text{s} - 846.0\,\text{s}}{846.0\,\text{s}} \cdot 100 \approx 9.6\%. \tag{4.9}$$

For the nonlinear model:

$$\Delta_{\text{nonlin}} = \frac{873.8\,\text{s} - 846.0\,\text{s}}{846.0\,\text{s}} \cdot 100 \approx 3.3\%. \tag{4.10}$$

The results show that the nonlinear model closely fits the real measurements, while the simpler linear model with optimized parameters also provides a good approximation. The deviations in the range of 3.3%–9.6% validate the applicability of both models for simulating battery energy consumption in industrial prediction and design processes.

5. Investigation of Sliding Mode Control in the Nonlinear Modeling of Battery-Powered Jigsaws

During the operation of battery-powered handheld jigsaws, load fluctuations and cutting disturbances significantly affect performance and energy consumption. Sliding Mode Control (SMC) offers a robust solution to these challenges by effectively handling disturbances and parameter variations. Selecting a higher observer time constant allows for reduced inrush current and controlled speed ramp-up. This strategy ensures stable operation, lower current stress, and extended battery runtime. The presented theoretical background is partly based on the works of [9] and [10], which provide a foundation for the detailed analysis and application of the proposed control method.

5.1. Application of the Theory to the Investigated Battery-Powered Jigsaw

The nonlinear electromechanical model of the jigsaw can be expressed in state-space form as:

$$\frac{\mathrm{d}}{\mathrm{d}t}\begin{bmatrix} q \\ i \\ \varphi_m \\ \omega \end{bmatrix} = \begin{bmatrix} 0 & 1 & 0 & 0 \\ 0 & -\frac{R_a+R_b}{L_a} & 0 & -\frac{k_e}{L_a} \\ 0 & 0 & 0 & 1 \\ 0 & a_{42}(\varphi_m) & 0 & a_{44}(\varphi_m) \end{bmatrix} \begin{bmatrix} q \\ i \\ \varphi_m \\ \omega \end{bmatrix} + \begin{bmatrix} 0 & 0 \\ \frac{1}{L_a} & 0 \\ 0 & 0 \\ 0 & b_{42}(\varphi_m) \end{bmatrix} \begin{bmatrix} v_{in}(t) \\ F_{saw} \end{bmatrix}, \tag{5.1}$$

where $v_{in}(t)$ is the motor input voltage and F_{saw} is the cutting force. The nonlinear coefficients describe the parameter-dependent dynamics of the mechanical subsystem, especially due to the scotch-yoke mechanism. To simplify the motor dynamics, it is considered that the mechanical time constant (T_m) is significantly greater than the electrical time constant (T_e):

$$T_e = \frac{L_a}{R_a + R_b}, \quad T_m = \frac{(R_a + R_b)J_{eq}}{k_e k_m}, \quad J_{eq} = J_m + J_k k_{mk}^2. \tag{5.2}$$

This allows the observer to be reduced to the mechanical subsystem, neglecting the influence of electrical dynamics [9–14].

5.2. Simulation Setup

The simulation system implemented in Simulink consists of four parallel sub-models, each representing different dynamic aspects of the jigsaw. The first block is a second-order

linear reference model serving as a baseline. The second block is a detailed nonlinear model of the cutting process without compensation, while the third block contains the compensated version of the same nonlinear model, where a first-order reference model improves system stability and dynamic response. The nonlinear model calculates the parameter-dependent dynamics based on output states, defining the motor and mechanical subsystem behavior. The compensated model uses a first-order reference observer to estimate motor angular velocity via a modified transfer function with a scaling factor.

5.2.1. Sliding Mode Simulation

In the Simulink-based simulation, the jigsaw's operation was modeled over a 3-second interval with a 10^{-6}-second integration step using the Euler method. The effect of sliding mode control was analyzed through angular velocity and current consumption. As shown in Figure 5.1, the uncompensated model rapidly reaches operational speed with a current spike, whereas sliding mode control yields a slower speed increase with significantly reduced current peak.

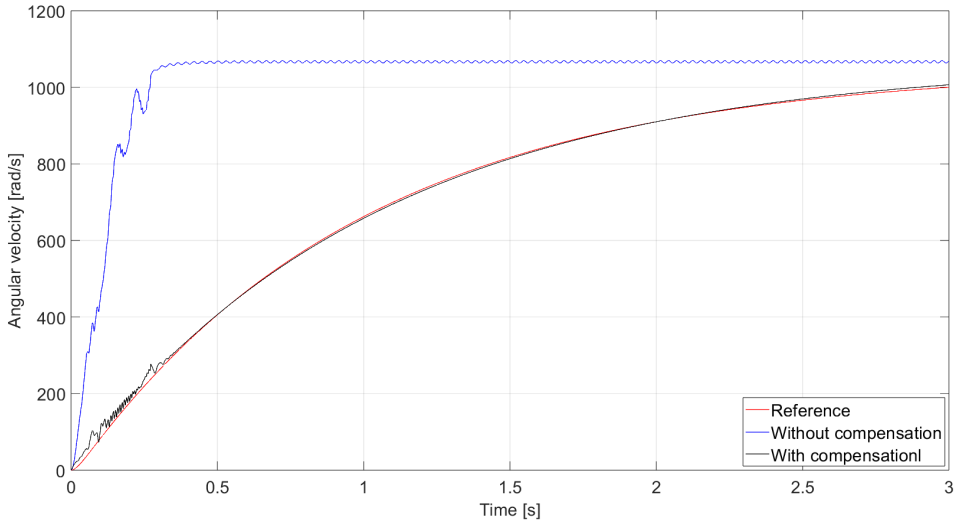

Figure 5.1: Angular velocity versus time.

5.2.2. Sliding Mode Simulation with Reduced-Order Observer

The reduced-order state observer employs a two-layer observation strategy. The first layer estimates key state variables (e.g., angular velocity, current), while the second compensates for nonlinear and under-modeled dynamics. The observer aims to provide stable and accurate state estimation while reducing high-frequency oscillations and estimation errors. Simulation results show that applying the reduced-order observer significantly improves angular velocity response (Figure 5.2), reduces peak current and oscillations. The comparison of output signals is shown in Figure 5.3, where the estimated angular velocity (blue) closely follows the nonlinear model's angular velocity (red), effectively suppressing oscillations.

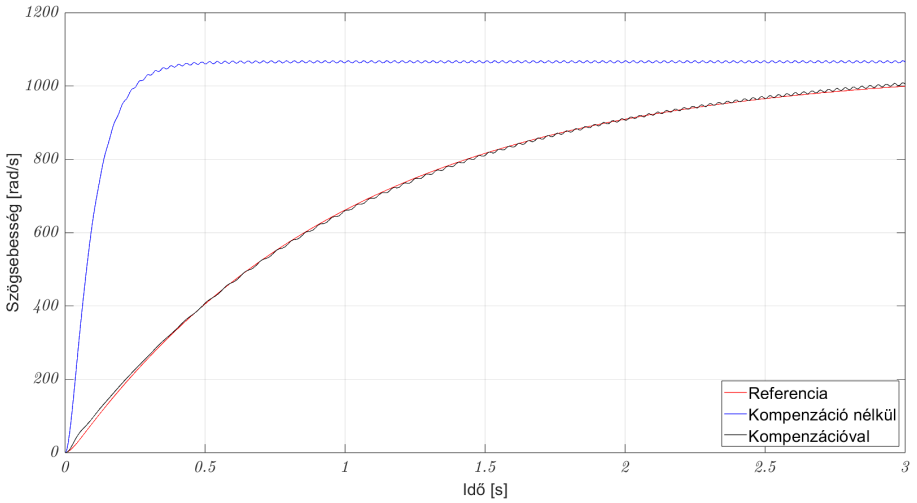

Figure 5.2: Angular velocity versus time with reduced-order observer.

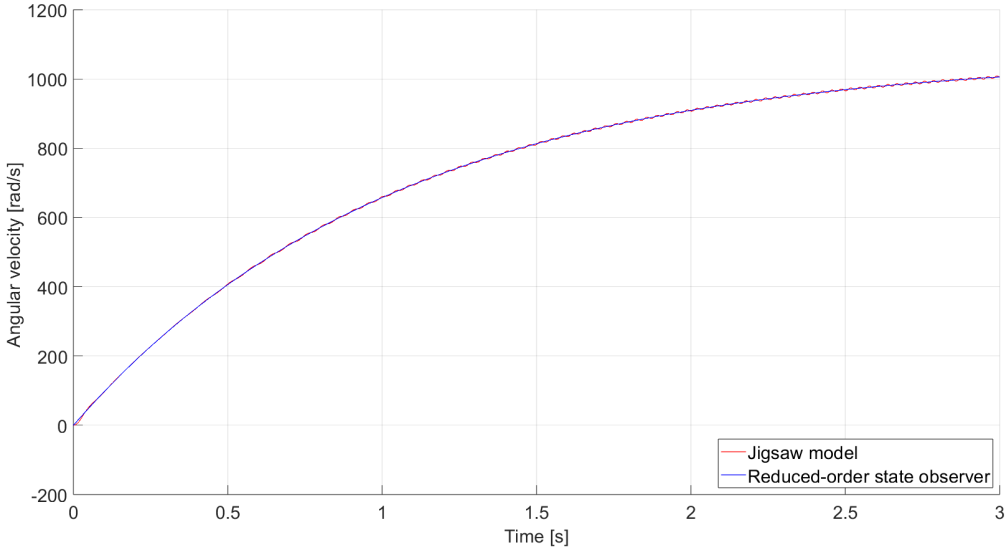

Figure 5.3: Difference between estimated and actual angular velocity.

In summary, the application of a reduced-order observer reduces oscillations in current and angular velocity, improves control accuracy, and increases system stability. The observer is particularly effective in compensating for under-modeled dynamics and non-linear mechanical effects, thereby contributing to longer service life and energy-efficient operation.

6. New Scientific Results

- T1. I designed a novel measurement system and developed a measurement method using Fourier transform analysis to determine the cutting force of a handheld jigsaw in real time. This method is capable of revealing the influence of the scotch yoke mechanism's angular velocity and the feed rate on the cutting force [S4].

- T2. Based on the measurements carried out using the developed system, I determined that the specific cutting force increases proportionally with the actual rotational speed of the jigsaw. For oak wood, a favorable operational range was identified between $n = 20{-}25\ \mathrm{s}^{-1}$ rotational speed and $v_f = 5{-}6\ \mathrm{mm\,s}^{-1}$ feed rate, where the specific cutting force falls between $4000\ \mathrm{N\,mm}^{-2}$ and $5200\ \mathrm{N\,mm}^{-2}$. These results support the implementation of load-dependent speed control and adaptive regulation [S4].

- T3. I described the cutting process of the jigsaw using a nonlinear model based on measured cutting force and a linear model with an optimized damping coefficient. The validity of these models was assessed through validation over a 50-second measurement period, covering more than 5% of the total simulation time. The reference operating time calculated based on motor current was 846 s, while the nonlinear model yielded 873.8 s and the linear model 926.96 s. The nonlinear model using real cutting force resulted in a 3.3% relative error, while the linear model showed a 9.6% error, indicating that the simplified model can also predict battery life with adequate accuracy [S5].

- T4. I designed a sliding mode-based, reduced-order, model reference robust controller with discontinuous feedback for the jigsaw described by a nonlinear state-space equation subjected to stochastic disturbances due to the cutting force. I proved the stability of the system and solved its reduced-order differential equation under ideal conditions using the theory of discontinuous differential equations [S6].

- T5. The controller presented in thesis T4 causes oscillations in real-world conditions due to unmodeled dynamics, potentially leading to equipment damage. To avoid such oscillations, I designed a reduced-order observer for the reduced-order model, which runs in the computer's memory. In this environment, the ideal sliding mode can be realized and numerically approximated without oscillations [S6].

7. Development Opportunities

The measurement system, modeling methodology, and control concept presented in the dissertation provide a starting point for deeper understanding and optimization of the operation of handheld jigsaws. Future developments may improve the system's accuracy, reliability, and generalizability in multiple directions.

From the perspective of improving the measurement system, enhancing its dynamic characteristics is particularly important. Experimental results have shown that negative cutting forces and oscillations partially result from elastic deformations in the bench and force measuring unit. To reduce these effects, it would be advisable to reinforce the construction and to experimentally identify, integrate into the model, and compensate for the elasticity and vibrational characteristics. A more precisely calibrated and damped system could contribute to a more reliable identification of the true physical background of cutting force fluctuations.

The effect of tool wear is currently estimated empirically, but for objective tracking, it would be advisable in the future to introduce sensor-supported automatic wear monitoring. Wear prediction could be carried out using frequency analysis of the cutting force or motor current and predictive methods, thereby improving maintenance scheduling and measurement consistency.

On the modeling side, it is justified to further refine the calculation of specific cutting force for multiple materials. The current studies provide detailed map diagrams for oak, but similar analyses should also be conducted for Metamid (PA6) and acacia wood to determine the ranges depending on angular velocity and feed rate. This would allow material-specific optimization and provide an answer to the reviewer's question about the extent to which the material type influences the reduction of motor angular velocity.

In terms of control, sliding mode control could be further developed toward adaptive or machine learning-based algorithms. Intelligent control could optimize operating parameters in real time based on cutting resistance and energy consumption, thus extending battery life and tool durability.

In summary, through the physical and software development of the measurement system, the expansion of material testing, and the implementation of automated evaluation, a complex, adaptive, and reliable system can be realized that also supports industrial applications of handheld jigsaws.

List of Publications Related to the Research Area

[S1] Apáti, Sándor; Hegedűs, György. "Investigation and Simulation of a Scotch Yoke Mechanism." *Multidiszciplináris Tudományok*, 13(2), pp. 144–152, 2023. DOI: 10.35925/j.multi.2023.2.13.

[S2] Apáti, Sándor; Hegedűs, György. "Szúrófűrész vizsgáló próbapad koncepcionális tervezése." *GÉP*, 74(4), pp. 13–16, 2023. (*in Hungarian*)

[S3] Apáti, Sándor; Hegedűs, György. "Electromechanical Model of Jigsaw." *Proceedings of the 11th International Conference on Advanced Technologies (ICAT'23)*, pp. 100–104, 2023. DOI: 10.58190/icat.2023.24.

[S4] Apáti, Sándor; Hegedűs, György; Hajdu, Sándor. "Semi-in-situ cutting force measurement of a jigsaw." *Results in Engineering*, 25, 104114, 2025. DOI: 10.1016/j.rineng.2025.104114.

[S5] Apáti, Sándor; Hajdu, Sándor; Hegedűs, György. "Simscape alkalmazása vágóerő modellezésére." In: Hegedűs, György; Rónai, László (szerk.) *Fiatal kutatók eredményei a Miskolci Egyetem Gépészmérnöki és Informatikai Karának Szerszámgépészeti és Mechatronikai Intézetében – 2024*, Miskolc-Egyetemváros, Magyarország: Miskolci Egyetem, Gépészmérnöki és Informatikai Kar, Szerszámgépészeti és Mechatronikai Intézet, 2024, pp. 68–75. (*in Hungarian*)

[S6] Apáti, Sándor; Hegedűs, György; Hajdu, Sándor; Korondi, Péter. "Investigation of Sliding Mode Control in the Nonlinear Modeling of Cordless Jigsaws." *Sensors*, 25(2), 456, 2025. DOI: 10.3390/s25020456.

References

[1] A. Naylor, P. Hackney, E. Clahr, Machining of wood using a rip tooth: Effects of work-piece variations on cutting mechanics, in: Conference: 20th International Wood Machining, 2011, p. 10.

[2] R. Pfeiffer, R. Collet, L. E. Denaud, G. Fromentin, Analysis of chip formation mechanisms and modelling of slabber process, Wood Science and Technology 49 (1) (2014) 41–58. doi:10.1007/s00226-014-0680-x.

[3] U. Oberst, The Fast Fourier Transform, SIAM Journal on Control and Optimization 46 (2) (2007) 496–540. doi:10.1137/060658242.

[4] P. Moradpour, K. Doosthoseini, F. Scholz, A. Tarmian, Cutting forces in bandsaw processing of oak and beech wood as affected by wood moisture content and cutting directions, European Journal of Wood and Wood Products 71 (6) (2013) 747–754. doi:10.1007/s00107-013-0734-z.

[5] P. Moradpour, F. Scholz, K. Doosthoseini, A. Tarmian, Measurement of Wood Cutting Forces during Bandsawing Using Piezoelectric Dynamometer, Drvna industrija 67 (1) (2016) 79–84. doi:10.5552/drind.2016.1433.

[6] V. Meulenberg, M. Ekevad, M. Svensson, O. Broman, Minor cutting edge force contribution in wood bandsawing, Journal of Wood Science 68 (1) (Mar. 2022). doi:10.1186/s10086-022-02023-8.

[7] N. Vorkapic, N. Slavkovic, B. Kokotovic, S. Zivanovic, Z. Dimic, Implementation of a cutting forces model through virtual simulation of machining process, International Journal of Advanced Manufacturing Technology 135 (2024) 3085–3099. doi:10.1007/s00170-024-14681-7.

[8] B. Zhang, C. Zhao, B. Wen, Dynamic cutting force measurement test and prediction of time series model for machine tools, Journal of Northeastern University (Natural Science) 40 (4) (2019) 521–526. doi:10.12068/j.issn.1005-3026.2019.04.013.

[9] K. . H. H. Korondi, P ; Young, Discrete-time sliding mode based feedback compensation for motion control, in: Proceedings. 1996 IEEE International Workshop on Variable Structure Systems.-VSS'96-, IEEE, 1996, pp. 127–131. doi:10.1109/VSS.1996.578577.

[10] N. Fink, G. Zenan, P. Szemes, P. Korondi, Comparison of direct and inverse model-based disturbance observer for a servo drive system, Acta Polytechnica Hungarica 20 (4) (2023). doi:10.12700/APH.20.4.2023.4.12.

[11] Z. Guo, P. Korondi, P. T. Szemes, Bond-graph-based approach to teach pid and sliding mode control in mechatronics, Machines 11 (10) (2023) 959. doi:10.3390/machines11100959.

[12] C. Peris, M. Norton, S. Y. Khoo, Variations in finite-time multi-surface sliding mode control for multirotor unmanned aerial vehicle payload delivery with pendulum swinging effects, Machines 11 (9) (2023) 899. doi:10.3390/machines11090899.

[13] Y. Zhang, H. Lu, M. Li, X. Liu, Speed regulation and optimization of sensorless system of permanent magnet synchronous motor, Machines 11 (6) (2023) 656. doi:10.3390/machines11060656.

[14] P. Korondi, N. Fink, R. Mikuska, P. T. Szemes, C. Kézi, I. Kocsis, On the mathematical background of sliding mode-based friction compensation of a micro-telemanipulation system, Mathematics 12 (20) (2024) 3182. doi:10.3390/math12203182.